AN EXPERIMENTAL STUDY OF THE STEADY NATURAL CONVECTION IN A HORIZONTAL ANNULUS WITH IRREGULAR BOUNDARIES*

CONF-800723--1

R. D. Boyd
Fluid & Thermal Sciences Department
Sandia Laboratories†
Albuquerque, NM 87185

MASTER

ABSTRACT

The natural convective heat transfer across an annulus with irregular boundaries was studied using a Mach-Zehnder interferometer. The annulus was formed by an inner hexagonal cylinder and an outer concentric circular cylinder. This configuration models, in two dimensions, a liquid metal fast breeder reactor spent fuel subassembly inside a shipping container. During the test, the annulus was filled with a single gas, either neon, air, argon, krypton, or xenon, at a pressure of about 0.5 MPa.

From temperature measurements, both local and mean Nusselt numbers (Nu_Δ) at the surface of the inner cylinder were evaluated, with the mean Rayleigh number ($\overline{Ra}_\Delta$) varying from 4.54×10^4 to 0.915×10^6 (Δ is the local gap width). The data correlation for the mean Nusselt and Rayleigh numbers is given by $\overline{Nu}_\Delta = 0.183\ \overline{Ra}_\Delta^{0.310}$.

*This work was supported by the U. S. Department of Energy under contract DE-AC04-76DP00789.

†A U. S. Department of Energy facility.

NOMENCLATURE

g = gravitational acceleration

$\overline{Nu}$ = mean Nusselt number defined in Eq. (2)

Nu_Δ = local Nusselt number, $\partial T/\partial r\big|_{r=r_i} \Delta/(T_i - T_o)$

$\overline{Nu}_\Delta$ = mean value of Nu_Δ, obtained over the applicable interval for θ

$\overline{Nu}_{\Delta c}$ = correction included in $\overline{Nu}_\Delta$ due to conduction heat transfer through the supporting stand for the hexagonal cylinder

p = pressure of the gas in the annulus

P = ratio of the annulus gas pressure to the pressure at standard conditions

r = radial coordinate measured from the center of the inner cylinder

Ra_m = mean Rayleigh number defined in Eq. (2)

Ra_Δ = local Rayleigh number, $[g\beta P^2(T_i - T_o)\Delta^3]/\alpha\nu$

$\overline{Ra}_\Delta$ = mean value of Ra_Δ, obtained over the applicable interval for θ

T = temperature

α = thermal diffusivity

β = thermal coefficient of volumetric expansion

Δ = local annulus gap width , $(r_o - r_i)$

ε = fringe shift or order number

θ = angular coordinate measured from the top of the annulus

ν = kinematic viscosity

Subscripts

i = evaluated at the inner cylinder

0 = evaluated at the outer cylinder

AN EXPERIMENTAL STUDY OF THE STEADY NATURAL CONVECTION IN A HORIZONTAL ANNULUS WITH IRREGULAR BOUNDARIES

Introduction

Natural convection heat transfer is an important mechanism of energy transfer in many practical systems. Numerous applications are found in energy storage, reactor safety, passive solar systems, and reactor waste transport and storage.

This experimental study deals with the measurement of the heat transfer across a horizontal annulus which is formed by an inner hexagonal cylinder and an outer concentric circular cylinder. The geometry simulates in two dimensions a liquid metal fast breeder reactor radioactive fuel subassembly inside a shipping container. This geometry is also similar to a radioactive fuel pin inside a horizontal reactor subassembly.

The objective of the experiments is to measure the local and mean heat transfer coefficients at the surface of the inner hexagonal cylinder.

Very little work has been done on the heat transfer by natural convection in a horizontal annulus formed by an inner hexagonal cylinder and an outer circular cylinder. Klima [1]*

*Numbers in brackets designate references at end of paper.

measured the overall heat transfer coefficients due to natural and forced convection using argon, helium, and liquid sodium. Allen, et al [2] used the correlation technique of Itoh, et al [3] to correlate the data produced by Klima. Schimmel [4] made a demonstration interferogram which displayed conduction-dominated heat transfer, using a holographic interferometer. Gartling [5] made two-dimensional numerical finite element predictions for the case of a hexagonal cylinder resting on the bottom of an outer circular cylinder. The natural convective flow regime studied by Gartling was near the transition between thermal conduction and laminar transport.

The natural convective flow in a horizontal annulus formed by an inner hexagonal cylinder and an outer concentric circular cylinder is similar to the natural convection flow in the annulus formed by concentric circular cylinders. However, the presence of corners and flat surfaces in the former annulus make the two cases different enough to warrant additional study.

Numerous authors, e.g. [6 - 15], have studied the natural convective flow between horizontal concentric cylinders. Kuehn [6] and Kuehn and Goldstein [7-8] have reviewed the literature thoroughly. Using a Mach-Zehnder interferometer, they examined experimentally and numerically the local and mean heat transfer coefficients for both concentric and eccentric cylinders. Their experimental results covered a range of the Rayleigh number (based on the gap width, Δ) of $2.2 \times 10^2 \leq Ra_\Delta \leq 7.7 \times 10^7$. Grigull and Hauf [9], using a Mach-Zehnder interferometer,

presented experimental results of the Nusselt number (Nu_Δ) as a function of the Grashof number (Gr_Δ, for $10^2 < Gr_\Delta < 10^6$) and the ratio of the gap width to the diameter of the inner cylinder. They also presented, using smoke dispersion, two-dimensional photographs of the streamlines of the flow fields. Lis [10] pressurized the annulus fluid to achieve turbulent heat transfer, with the Rayleigh number being as high as 10^{10}. Many other studies and correlational analyses, e.g. [11-15], have been conducted on the natural convective transport between concentric cylinders.

Experimental Study

A 19.7 cm aperture Mach-Zehnder interferometer (see Fig. 1) was used to record the steady two-dimensional temperature distribution in the horizontal annulus formed by an inner hexagonal cylinder (hex) and an outer concentric circular cylinder. The light source for the interferometer was a 50.0 mW He-Ne CW laser. The data records (or interferograms) were analyzed to yield the local temperature distribution. The local or mean heat flux was obtained from the temperature distributions.

Interferometric techniques are ideal for both time-averaged and instantaneous heat transfer measurements in transparent media because: (1) the test medium is not perturbed by an external probe; (2) the interferometer has essentially no inertia; and (3) permanent whole-field quantitative data records are obtained. The disadvantages are: (1) large optical systems are usually expensive; and (2) the interferometer must be stable and vibration isolated.

As noted previously, for concentric cylinders the Nusselt number can be directly correlated to the Rayleigh number and the ratio of the radii. However, since a large number of experiments are required to produce such results for the hex inside the circular cylinder, it was decided to conduct all experiments using prototypic cross-sectional dimensions.

The present study is Phase I (pressure $\sim$ 0.5 MPa) of a broader heat transfer study in which the annulus pressure, gas molecular weight (helium, neon, air, argon, krypton, or xenon), and the temperature difference are experimental parameters which are used to achieve large differences, from test to test, in the mean Rayleigh number.

Apparatus

The test cell, which is positioned in one leg of the interferometer, is shown in Fig. 2. The test cell consists of an inner hex which is seated on a small stand and concentrically located inside a horizontal circular cylinder. Because of the size of the test cell, only about half of its cross section was illuminated. This is sufficient since the annulus flow is symmetrical about a vertical plane passing through the center of the cell.

The inner hex is orientated with two flat sides horizontal. The hex, which was fabricated from solid aluminum (7075, T651) stock, is 14.0 cm long and has six sides which are 6.4 cm in

width. This cylinder was heated by a circular cylindrical resistive heater (2.5 cm in diameter) which was located in the center of the hex. Four thermocouples were positioned just below ($\sim$ 3 mm) the surface of four of the six sides of the hex (θ = 0, $\frac{\pi}{3}$, $\frac{2\pi}{3}$ and $\sim \pi$rad). Note that θrad at the top of the hex. On a given hex side, the thermocouples were located at axial positions of 2.5, 4.8, 6.4, and 7.9 cm from one end of the cylinder. All thermocouple and heater electrical leads were passed through a slot located near the rear of the test cell.

The outer circular cylinder, also aluminum, is 20.3 cm long and has an inside diameter of 19.0 cm. Three thermocouples were located in a vertical plane passing through the center of the length of the test cell and along the surface of the outer cylinder at θ = 0, $\pi/3$, and $2\pi/3$. Inside the cross section of this cylinder were located circumferential channels (see Fig. 2b) through which flowed a coolant, ethylene glycol. The coolant was maintained at an isothermal temperature by a recirculating constant temperature bath. The flow lines for the coolant were coiled to reduce vibration transmission to the optical table. The outer surface channels were insulated with $\sim$1.2 cm of min-K insulation. The thermocouple data were recorded to within $\sim$0.05 K.

The test cell windows are made of fused silica (grade A) and have a wedge angle of less than 24.2 urad. The windows are 25.4 cm in diameter and 4.5 cm thick.

The principles of adjustment and operation of the Mach-Zehnder interferometer have been described by many authors, e.g. [16-18].

Procedure

Prior to all experimental runs, the interferometer and test cell alignment were checked and corrected. The alignment of the auxiliary optical equipment (i.e., everything downstream of the second beam splitter of the interferometer) was also checked. Appropriate adjustments were made to the imaging system so that the midplane, along the axis, of the test cell was imaged onto the observation screen. The test cell was then filled (to $\sim$ 0.07 MPa) with research-grade gas and subsequently evacuated. This fill-evacuate sequence was repeated at least four times. The annulus was then pressurized to a predetermined level. Finally, the entire system was left overnight so that a state of thermal equilibrium could be attained.

An isothermal infinite fringe adjustment was made to the interferometer. The alignment of the test cell was again checked. Photographs of the infinite fringe setting were taken so that the uniformity of the interference field and the optical adjustments could be evaluated. The predetermined recirculating bath temperature was set. Temperatures in the interferometer's reference and test cell legs were recorded. The power for the resistive heaters was set to a predetermined level. The apparatus was left and allowed to reach a steady state, which usually occurred from six to eleven hours after the experimental runs began.

After a steady state was attained, the initial data aquisition was begun. The system was assumed to exist at a steady state when the test cell temperature changes were less than 0.10 K. The data acquisition included recording the local barometric pressure, the reference and test cell temperatures, the circulating bath's temperature, the test cell gage pressure, and the power generation level of the resistive heater. Soon after these measurements were recorded, a number of interferograms were recorded. The experimental parameters were controlled to match the characteristics of Polaroid 105 p/n film; no more than approximately ten fringes appeared on any particular interferogram. The camera used was a Rolleiflex (model SL-66) with a 150 mm lens. Typical exposures and f-stop settings were 0.25 s and f-2.8, respectively.

Local temperature distributions were obtained from each interferogram along seven ($\theta = \pi/6$, $\pi/3$, $\pi/2$, $2\pi/3$, $5\pi/6$, $\sim \pi/18$, and $\sim\pi$ rad) radial lines across the annulus. The measurement of the fringe location from the negatives was made using a tool-maker's microscope. Such measurements were made starting at the surface of the hex. The local temperature was obtained by relating the fringe order number to the corresponding index of refraction change, surface temperature of the hex, the local barometric pressure, test cell gage pressure, the reference leg temperature and properties of the test and reference gases. The

three data points nearest the surface of the hex were fitted to a straight line. This provided a good estimation of the temperature gradient and, hence, the local heat flux (or Nusselt number) at the surface of the hex. The Rayleigh number and the temperature difference across the annulus were evaluated for each angular position. At each radial position, all gas properties were evaluated at the arithmetic mean (or bulk) temperature. The mean Nusselt and Rayleigh numbers were obtained by integrating the respective quantity over the total interval of the angular distribution. It should be emphasized that included in the definition of the local Nusselt and Rayleigh numbers is the effect of the angular variation in the annulus gap width, Δ.

Corrections were made to the mean Nusselt number due to conduction through the aluminum stand which supported the hex.

As will be seen later, extraneous (or secondary) fringes were superimposed on the interferogram. These fringes were due to the interference of the front and back surface reflections from the beam splitter upstream of the basic interferometer components. A polarizer was used to reduce the contrast of these secondary fringes in the annulus. Spatial filtering in the Fourier transform plane was attempted but the spatial separation of the secondary fringes from the zeroth order light was not great enough to make this completely effective. The combination of the polarizer, spatial filtering, and the interference of the test and reference legs of the interferometer reduced the contrast of the secondary fringes to a level where they were not a nuisance in evaluating the interferograms.

Results

The result of a particular experimental run is an interferogram which is a pattern of light and dark fringes (or lines). The fringes are associated with changes in the local index of refraction which is proportional to the local temperature in the annulus. The fringes, therefore, represent isotherms (in two dimensions), an example of which can be seen in Fig. 3 (argon gas, $Ra_\Delta = 2.0 \times 10^5$).

Inspection of Fig. 3 reveals some interesting characteristics about the two-dimensional temperature distribution in an annulus formed by a hexagonal cylinder (hex) inside a concentric circular cylinder. Boundary layer flows exist near the surfaces, i.e. adjacent to both the hexagonal and circular cylinders, of the annulus. In addition, the flow is partially turbulent and is characterized by the upper half of the annulus being an unsteady turbulent flow and the lower half being a steady laminar flow. This type of flow existed for all cases considered, i.e., for $\overline{Ra}_\Delta \geq 4.5 \times 10^4$. It should be noted that a similar partially turbulent flow exists at a higher mean Rayleigh number ($\sim 10^7$) for the annulus formed by concentric cylinders [7].

The inner thermal boundary layer adjacent to the hex increases, but not monotonically, in thickness (thermal diffusion) as it proceeds upward. The spacing of the isotherms decreases as the hex is approached from the normal direction. This implies that the corresponding temperature gradient or heat flux increases as the hex is approached. Further, as

the gas flows around the corner at $\theta = 90^{o}$ (horizontal mid-plane of the interferogram), the isotherms deflect towards the hex surface and, thereby, increase the local heat flux. As the gas continues to flow along the upper incline (near $\theta = 60^{o}$) of the hex, the thermal boundary layer diffuses and appears to become partially turbulent. It is interesting to note that the thermal boundary layer remains attached to the hex (for $\theta < 30^{o}$) after the momentum boundary layer separates at the upper corner ($\theta = 30^{o}$) of the hex. The separation of the momentum boundary layer is denoted in real-time observations by a number of thermal cells leaving the upper corner of the hex at a measurable rate.

The outer thermal boundary layer develops along the circular cylinder as the thermal plume flow (not seen in Fig. 3) leaves the hex near $\theta = 0^{o}$. The turbulence which developed in the inner boundary layer is transmitted via the plume to the outer cylinder. This turbulent character is denoted by the wave-like structure in the outer isotherm of this boundary layer. As the boundary layer continues to diffuse along the outer cylinder, the turbulent intensity is attenuated. Below the horizontal mid-plane of the annulus ($\theta = 90^{o}$), this boundary layer appears to be laminar.

An intermediate flow region exists between the two thermal boundary layers. The temperature in this region is stratified in the angular direction. There are inflections (or a reversal in the temperature gradient) of the temperature distributions along the radial direction at most angular locations. However, the temperature variation in this region is usually small.

The temperature distribution changes as the mean Rayleigh number increases or decreases relative to the distribution shown in Fig. 3 ($\overline{Ra}_\Delta = 2.0 \times 10^5$) for argon. As the Rayleigh number increases, the mean Nusselt number increases, as is seen in Fig. 4 ($\overline{Ra}_\Delta = 9.2 \times 10^5$). The increase in the Nusselt number compared to that in Fig. 3 is manifested by the reduced spacing between the isotherms (or fringes) in the inner and outer boundary layers. There is also a noticeable increase in the turbulent structure in the upper half of the annulus. This is more apparent during real-time observations. The thermal field in the lower half of the annulus still appeared to be laminar.

When the Rayleigh number is decreased to $\overline{Ra}_\Delta = 4.5 \times 10^4$ (Fig. 5), another extreme in the thermal distribution is apparent. The Nusselt number is reduced, as is recognizable by the increased spacing between the isotherms. Although the turbulent intensity has decreased considerably from the former cases, there are noticeable fluctuations which are readily seen in real-time observations.

A thermal cell or an isotherm which closes on itself also appears in Fig. 5. The thermal cell is located just above the corner, which passes through the horizontal mid-plane of the annulus ($\theta = 90^o$). A subsequent experiment which is not reported in detail here was run using helium at a lower Rayleigh number than that shown in Fig. 5. When a steady state was achieved, a larger thermal cell appeared in approximately the same location as that seen in Fig. 5. This cellular configuration is a consequence of the interaction between the two thermal boundary layer flows on either side of the annulus. The interaction occurs as the two boundary layers diffuse thermal energy

at smaller values of the mean Rayleigh number. The appearance of the thermal cell is also dependent upon the ratio of the mean gap width to the mean radius of the inner boundary of the annulus. As this ratio increases, the thermal cell will disappear. More cells will likely appear when this ratio is decreased. The location of the corner at $\theta = 90^{\circ}$ is another factor which probably affects the appearance and location of the thermal cell(s).

The dimensionless radial temperature profiles for argon ($Ra_{\Delta} = 2.0 \times 10^{5}$) are presented in Fig. 6. These profiles are typical of many of those observed at other Rayleigh numbers. There are some similarities between the profiles for the annulus formed by concentric cylinders [8] and that formed by a hex placed inside a concentric circular cylinder. The boundary layer regions are well defined and the temperature inversions in the intermediate region are shown.

Detail inspection of the local Nusselt number (based on the local annulus gap width) distribution around the hex revelas some interesting differences from that found around the inner cylinder for the case of concentric cylinders. Figure 7 shows the angular distribution of the Nusselt number around the hex for air. One difference is observed as the inner boundary layer turns and proceeds around the corner at $\theta = 90$. For the case of the hex in the cylinder, the Nusselt number <u>decreases</u> at $\theta = 90^{\circ}$, <u>increases</u> at $\theta = 60^{\circ}$, and then decreases again as the boundary layer continues to diffuse. This pattern is repeated as the thermal boundary layer turns the corner at

$\theta = 30^{\circ}$, which is located near the top of the hex. Contrary to this, the local Nusselt number around the inner circular cylinder, for the concentric cylinder case, decreases monotonically as the fluid flows towards the top of the inner circular cylinder [8].

Since the field of view from the interferograms was limited, the location of the data points at $\theta \gtrsim 180^{\circ}$ and $\theta \gtrsim 10^{\circ}$ are approximate. The appearance of the supporting stand for the hex prevented observations to be made at $\theta = 180^{\circ}$. Rather, the observation was made near the corner at $\theta = 150^{\circ}$ and normal to the bottom horizontal surface of the hex. A similar approach was used for $\theta = 10^{\circ}$. In future experiments, the test cell will be moved so that the plume near $\theta = 0^{\circ}$ and $\sim 10^{\circ}$ can be observed. Future test cell modifications will include replacing the stand for the hex with small metal pins.

After the angular Nusselt number distribution around the hex was obtained for all gases, the mean Nusselt number was computed for each experimental run. The results for this mean Nusselt number ($\overline{Nu}_{\Delta}$) were plotted, in Fig. 8, as a function of the mean Rayleigh number ($\overline{Ra}_{\Delta}$) (see Table I for more detail). The characteristic length used for the local Rayleigh number was also the local annulus gap width. The mean Rayleigh number was computed from the angular Rayleigh number distribution. Using a linear regression analysis, it is found that the data in Fig. 8 can be described by

$$\overline{Nu}_{\Delta} = 0.183\ \overline{Ra}_{\Delta}^{0.310} \quad , \tag{1}$$

where

$$\overline{Nu}_{\Delta i} = \frac{1}{\pi}\int_0^{\pi} Nu_{\Delta} d\theta;\ \overline{Ra}_{\Delta} = \frac{1}{\pi}\int_0^{\pi} Ra_{\Delta} d\theta$$

$$\overline{Nu}_{\Delta} = \overline{Nu}_{\Delta i} - \overline{Nu}_{\Delta c};\ Nu_{\Delta} = \left.\frac{\partial T}{\partial r}\right|_{r=r_i} \frac{\Delta}{(T_i - T_o)};\ \text{and}$$

$$Ra_{\Delta} = \frac{g\beta P^2 (T_i - T_o)\Delta^3}{\alpha\nu} .$$

A bar over a quantity denotes the mean value of that quantity. In the expression $\overline{Nu}_{\Delta c}$ is a correction to the mean Nusselt number due to conduction heat transfer through the supporting stand for the hex. This correction term ranged from 0.8 to 3%.

The correlation technique given by Itoh, et al [3] has been applied to the annulus formed by concentric circular cylinders. This technique has been demonstrated to correlate previous data for laminar natural convective flow between concentric cylinders. The correlation is given by

$$\overline{Nu} = 0.20\ Ra_m^{0.25}\ , \text{ where} \qquad (2)$$

$$\overline{Nu} = \frac{r_o}{\Delta}\ ln\left(\frac{r_o}{r_i}\right)\ \overline{Nu}_{\Delta}, \text{ and } Ra_m = \left[\frac{(r_o r_i)^{0.5}}{\Delta}\ ln\left(\frac{r_o}{r_i}\right)\right]^3 Ra_{\Delta} .$$

There is an apparent difference between the annulus formed by a horizontal hexagonal cylinder inside a concentric circular cylinder and the annulus formed by horizontal concentric cylinders. However, for correlational purposes, if the hex is replaced by a circular cylinder with the same surface area, the correlation of Itoh, et al [3] may be applied. It should be pointed out that the coefficient, 0.2, will probably not be applicable for the annulus formed by a hex inside a concentric circular. The resulting

correlation is given by

$$\overline{Nu} = 0.436\ Ra_m^{0.25} \quad . \qquad (3)$$

However, it should be noted that Eq. (1) correlates the data much better than Eq. (3). A better correlation can be obtained for $\overline{Nu}$ in terms of Ra_m if the exponent of Ra_m is assumed not to equal 0.25.

Finally, there were no temperature variations measured at the surface of and along the length of the hex. This implied that the annulus flow, over most of the length of the hex, was two-dimensional. In addition, the temperature difference across the annulus was kept to a minimum so that refraction effects were minimized. However, since the length of the hex was shorter than the inside length of the test cell, end effects (although small) were not minimized. In future experiments, the length of the hex will extend along the entire inside length of the test cell.

Conclusions

The results of an experimental study of the steady natural convection in a horizontal annulus formed by an inner hexagonal cylinder and an outer concentric circular cylinder have been presented. The quantities measured include temperature distributions, and local and mean Nusselt numbers. During a given experimental run, the annulus was filled with either neon, air, argon, krypton, or xenon gas.

The results of the experimental runs were interferograms which were analyzed to give the temperature distributions across the annulus.

For relatively small Rayleigh numbers ($Ra_\Delta \geq 4.5 \times 10^4$), the boundary layer flow along the upper half of the inner hexagonal cylinder becomes turbulent. This turbulence is transported to the outer cylinder where it is damped as the outer boundary layer diffuses. This results in the upper half of the annulus having an unsteady turbulent flow and the lower half having an apparent steady laminar flow. The existence of the corners of the inner hexagonal cylinder, when compared with an inner circular cylinder, enhances the mean heat transfer.

Acknowledgements

The author gratefully acknowledges the efforts of W. P. Schimmel who ordered most of the equipment for the interferometer, and who, along with Jose Suazo, designed the test cell.

References

1. Klima, B. B., "LMFBR Spent Fuel Transport: Single Assembly Heat Transport Test," ORNL-TM-4936 (Oak Ridge National Lab., Tennessee, 1975).
2. Allen, G. C., et al, "Conceptual Design for LMFBR Spent Fuel Shipping Casks," SAND77-1483 (Sandia Laboratories, Albuquerque, NM, 1978).
3. Itoh, M., Nishiwaki, N., and Hirata, M., "A New Method for Correlating Heat-Transfer Coefficients for Natural Convection in Horizontal Cylindrical Annuli," International Journal of Heat and Mass Transfer, Vol. 13, pp. 1364-1368 (1970).
4. Schimmel, W. P., Jr., "An Optical Measurements Laboratory for Determining Heat Transfer Coefficients," SAND76-0162 (Sandia Laboratories, Albuquerque, NM, 1976).
5. Gartling, D. K., "Convective Heat Transfer Analysis by the Finite Element Method," Computer Methods in Applied Mechanics and Engineering, Vol. 12, No. 3, pp. 365-382 (December 1977).
6. Kuehn, T. H., "Natural Convection Heat Transfer from a Horizontal Circular cylinder to a Surrounding Cylindrical Enclosure," PhD Dissertation, University of Minnesota, 1976.
7. Kuehn, T. H. and Goldstein, R. J., "An Experimental Study of Natural Convection Heat Transfer in Concentric and Eccentric Horizontal Cylindrical Annuli," Journal of Heat Transfer, Vol. 100, pp. 635-640 (1978).

8. Kuehn, T. H. and Goldstein, R. J., "An Experimental and Theoretical Study of Natural Convection in the Annulus between Horizontal Concentric Cylinders," Journal of Fluid Mechanics, Vol. 74, Part 4, pp. 695-719 (1976).

9. Grigull, U. and Hauf, W., "Natural Convection in Horizontal Cylindrical Annuli," Third International Heat Transfer Conference (Chicago), p. 182-195 (1966).

10. Lis, J., "Experimental Investigation of Natural Convection Heat Transfer in Simple and Obstructed Horizontal Annuli," Third International Heat Transfer Conference (Chicago), p p. 196-204 (1966).

11. Kuehn, T. H. and Goldstein, R. J., "Correlating Equations for Natural Convection Heat Transfer betweeen Horizontal Circular Cylinders," International Journal of Heat and Mass Transfer, Vol. 19, p. 1127-1134 (1976).

12. Raithby, G. D. and Hollands, K.G.T., "A General Method of Obtaining Approximate Solutions to Laminar and Turbulent Free Convection Problems," Advances in Heat Transfer, Vol. 11, p. 265-315 (1975).

13. Charrier-Mojtabi, M. C., Mojtabi, A, and Caltagirone, J. P., "Numerical Solution of a Flow due to a Natural Convection in Horizontal Cylindrical Annulus," Journal of Heat Transfer, Vol. 101, p. 171-173 (1979).

14. Patanker, S. V., Ivanovic, M., and Sparrow, E. M., "Analysis of Turbulent Flow and Heat Transfer in Internally Finned Tubes and Annuli," Journal of Heat Transfer, Vol. 101, p. 29-37 (1979).

15. Van De Sande, E. and Hamer, B.J.G., "Steady and Transient Natural Convection in Enclosures between Horizontal Circular Cylinders (Constant Heat Flux)," International Journal of Heat and Mass Transfer, Vol. 22, p. 361-370 (1979).

16. Hauf, W. and Grigull, U., "Optical Methods in Heat Transfer," Advances in Heat Transfer, Vol. 6, p. 133-366, Academic Press, New York, NY (1970).

17. Eckert, E.R.G. and Goldstein, R. J., Measurements in Heat Transfer, 2nd Ed., p. 241-293, New York, NY (1976).

18. Merzkirch, W., Flow Visualization, p. 62-184, Academic Press, New York, NY (1974).

Figure Captions

Fig.	Caption
1	The Mach-Zehnder Interferometer (45^{o}) Used to Experimentally Record the Two-Dimensional Temperature Distribution
2	The Test Cell with the Annulus Formed by an Inner Hexagonal Cylinder inside an Outer Concentric Circular Cylinder.
3	An Interferogram Showing the Two-Dimensional Isotherms in the Annulus Formed by an Inner Hex and an Outer Concentric Circular Cylinder. Gas-Argon; $\overline{Ra}_{\Delta} = 2.0 \times 10^{5}$; Length of Hex Sides - 7.332 cm.
4	An Interferogram Showing the Two-Dimensional Isotherms in the Annulus Formed by an Inner Hex and an Outer Concentric Circular Cylinder. Gas-Xenon; $\overline{Ra}_{\Delta} = 9.2 \times 10^{5}$; Length of Hex Sides - 7.332 cm.
5	An Interferogram Showing the Two-Dimensional Isotherms in the Annulus Formed by an Inner Hex and an Outer Concentric Circular Cylinder. Gas-Neon; $\overline{Ra}_{\Delta} = 4.5 \times 10^{4}$; Length of Hex Sides - 7.332 cm.

Figure Captions (continued)

Fig.	Caption
6	Dimensionless Radial Temperature Distributions at Selected Angular Locations. Gas-Argon; $\overline{Ra}_{\Delta} = 2.0 \times 10^5$.
7	Angular Distribution of the Nusselt Number at the Surface of the Hex. Gas-Air; $Ra_{\Delta} \gtrsim 1.4 \times 10^5$.
8	Experimental Results of the Mean Nusselt Number ($\overline{Nu}_{\Delta}$) as a Function of the Mean Rayleigh Number ($\overline{Ra}_{\Delta}$) for the Annulus Formed by an Inner Hex inside a Concentric Circular Cylinder.

TABLE 1

SUMMARY OF EXPERIMENTAL RESULTS*

Gas (Molecular Weight)	Test Cell Pressure, p (MPa)	Mean Temperature Difference, $\overline{\Delta T}$ (K)	Mean Rayleigh Number, $\overline{Ra}_{\Delta} \times 10^{-4}$	Mean Nusselt Number, $\overline{Nu}_{\Delta}$	Mean Rayleigh Number, $Ra_m \times 10^{-4}$	Mean Nusselt Number, $\overline{Nu}$	Local Barometric Pressure (MPa)	Temperature** Difference (K) for $\varepsilon = 1$ and P = 0.507 MPa
Neon (20.2)	0.507	14.4	4.54	4.99	3.97	5.62	0.0857	3.16
Air (29.0)	0.532	4.7	13.65	7.33	11.97	8.06	0.0836	0.673
Argon (39.9)	0.532	5.1	20.04	7.63	17.53	8.22	0.0839	0.741
Krypton (83.7)	0.525	2.8	33.70	10.14	29.48	11.34	0.0854	0.493
Xenon (131.3)	0.521	2.4	91.47	12.55	79.83	14.00	0.0834	0.300

* The reference gas in the reference leg of the interferometer was air.

** $\varepsilon \equiv$ fringe shift or order number resulting from a specified temperature difference.

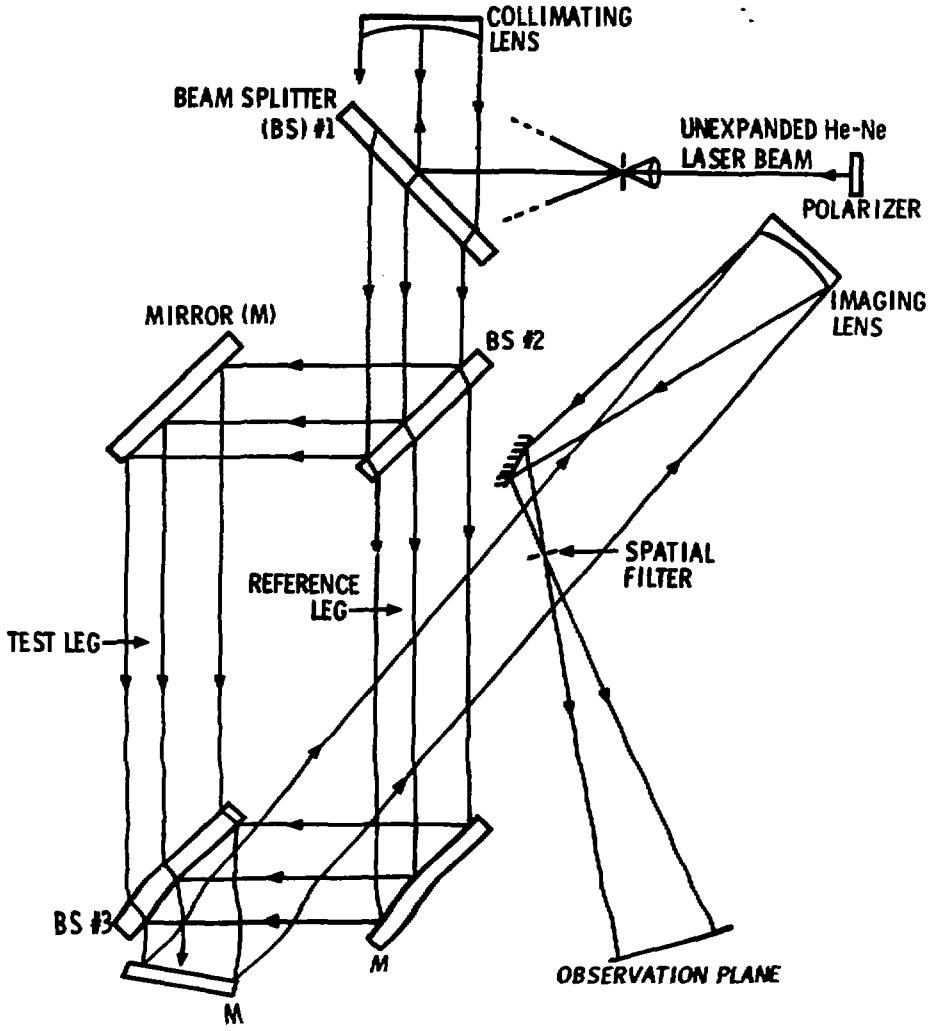
COLLIMATING LENS
BEAM SPLITTER (BS) #1
UNEXPANDED He-Ne LASER BEAM
POLARIZER
IMAGING LENS
MIRROR (M)
BS #2
SPATIAL FILTER
REFERENCE LEG
TEST LEG
BS #3
M
M
OBSERVATION PLANE

FIGURE 1

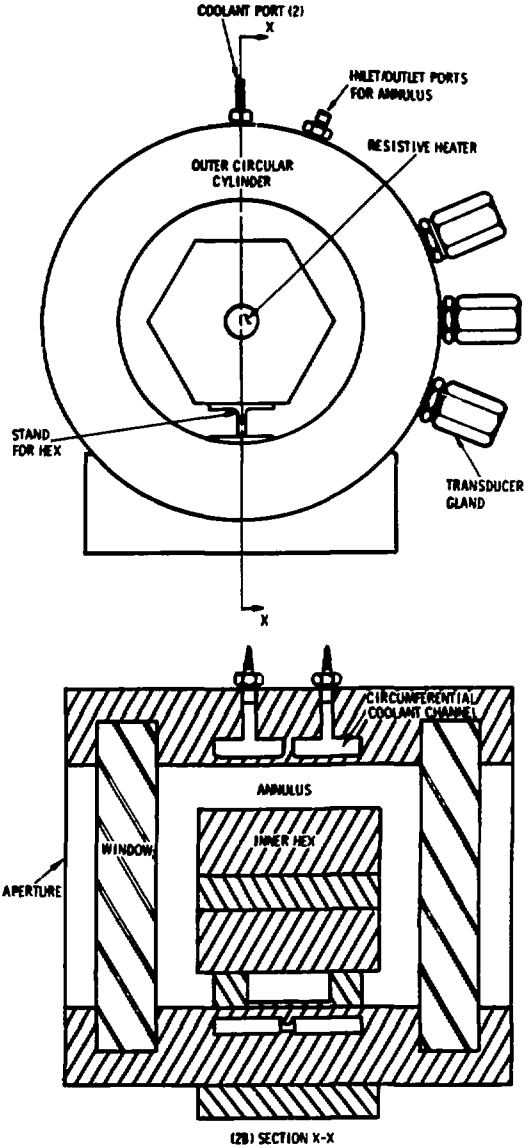
COOLANT PORT (2)
X
INLET/OUTLET PORTS FOR ANNULUS
RESISTIVE HEATER
OUTER CIRCULAR CYLINDER
STAND FOR HEX
TRANSDUCER GLAND
X
CIRCUMFERENTIAL COOLANT CHANNEL
ANNULUS
INNER HEX
WINDOW
APERTURE
(2B) SECTION X-X

FIGURE 2

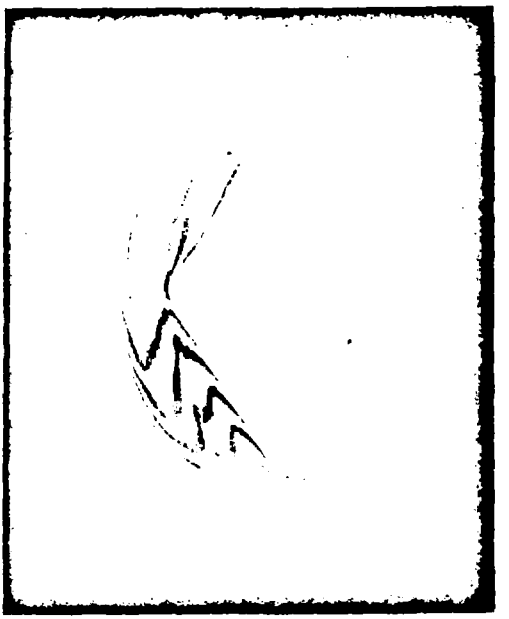

FIGURE 3

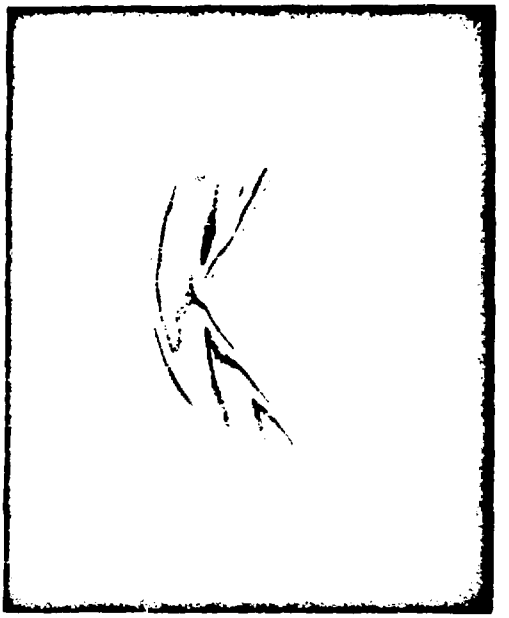

FIGURE 5

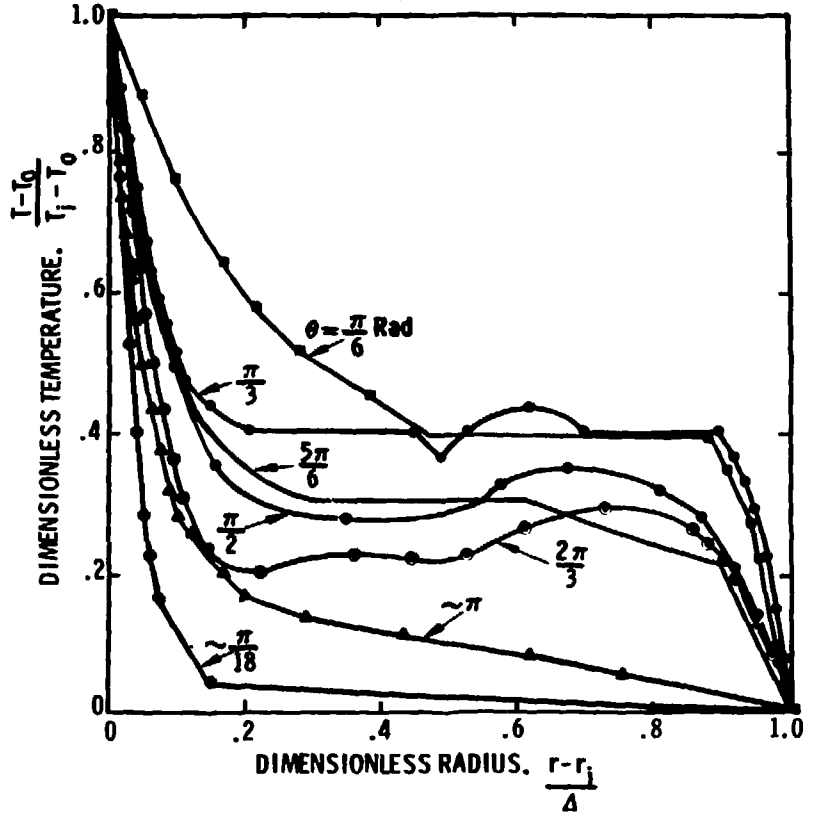
1.0
.8
.6
.4
.2
0
0
.2
.4
.6
.8
1.0
DIMENSIONLESS TEMPERATURE. $\frac{T-T_0}{T_j-T_0}$
DIMENSIONLESS RADIUS. $\frac{r-r_j}{\Delta}$
$\theta=\frac{\pi}{6}$ Rad
$\frac{\pi}{3}$
$\frac{5\pi}{6}$
$\frac{\pi}{2}$
$\frac{2\pi}{3}$
$\sim\pi$
$\sim\frac{\pi}{18}$

FIGURE 6

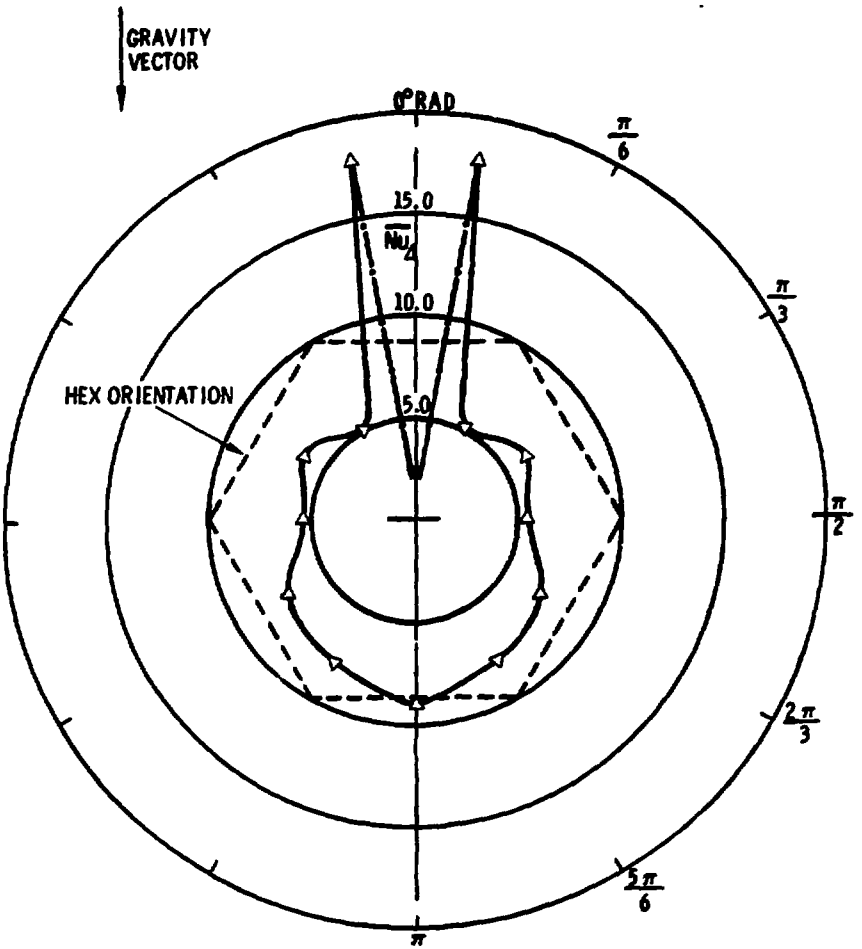
GRAVITY VECTOR
0° RAD
π/6
π/3
π/2
2π/3
5π/6
π
15.0
$\overline{Nu}_d$
10.0
5.0
HEX ORIENTATION

FIGURE 7

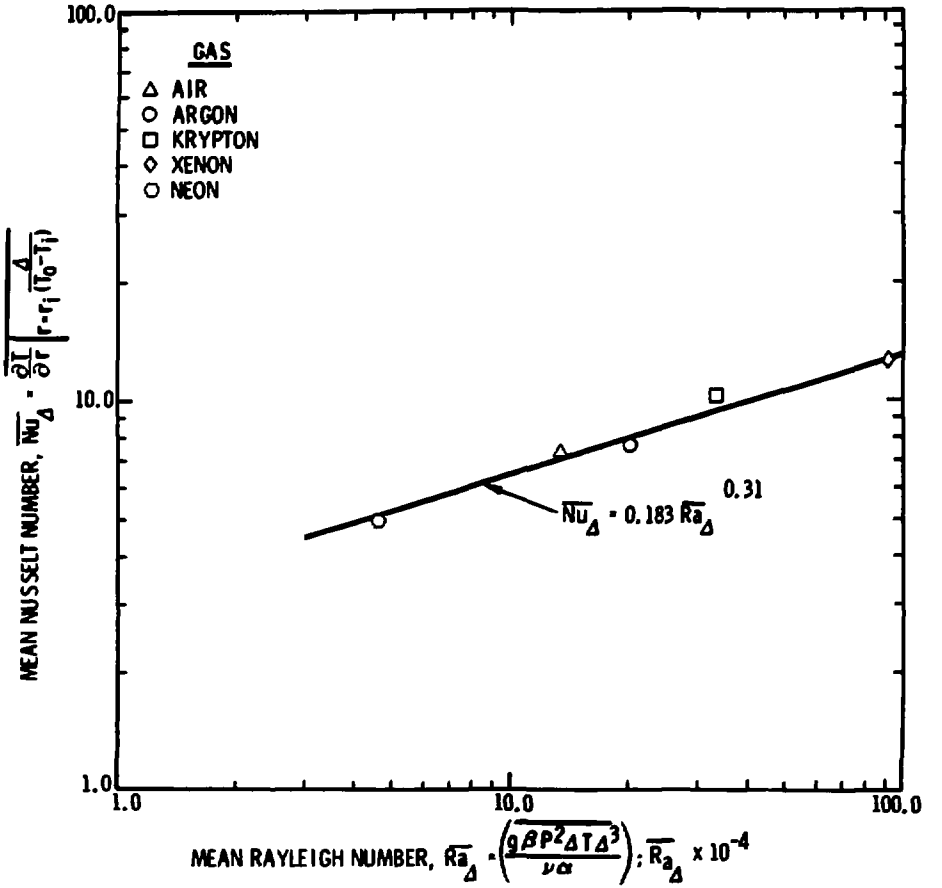
100.0
10.0
1.0
1.0
10.0
100.0
GAS
AIR
ARGON
KRYPTON
XENON
NEON
$\overline{Nu}_\Delta = 0.183\,\overline{Ra}_\Delta^{0.31}$
MEAN NUSSELT NUMBER, $\overline{Nu}_\Delta = \overline{\frac{\partial T}{\partial r}\left[r-r_i\,\frac{\Delta}{(T_o-T_i)}\right]}$
MEAN RAYLEIGH NUMBER, $\overline{Ra}_\Delta = \left(\overline{\frac{g\beta P^2 \Delta T \Delta^3}{\nu\alpha}}\right) : \overline{R}_{a_\Delta} \times 10^{-4}$

FIGURE 8